Theor Chem Acc (2011) 130:439–448
DOI 10.1007/s00214-011-1020-y

REGULAR ARTICLE

QM/MM investigation of the degradation mechanism of the electron-transporting layer

Toshio Asada · Kenichi Ohta · Takeshi Matsushita · Shiro Koseki

Received: 28 February 2011 / Accepted: 9 August 2011 / Published online: 31 August 2011

Abstract The mechanism of charge transfer among tris(8-hydroxyquinolinate)aluminum (Alq_3) molecules in the electron-transporting layer (ETL) under amorphous conditions was theoretically investigated using both quantum mechanical/molecular mechanical (QM/MM) calculations and molecular dynamics (MD) simulations. The rate constant of the electron transfer was estimated for the equilibrated structure taken from the QM/MM MD simulations, based on the hopping model and Marcus theory. It was found that the coordination of a $(LiF)_4$ cluster in ETL drastically lowers the energy of the lowest unoccupied molecular orbital in the Alq_3 molecule. The small rate constant, namely the slow charge mobility, in ETL is believed to be causally related to the low-lying delocalized unoccupied molecular orbital of Alq_3 coordinated by the $(LiF)_4$ cluster. The results suggest that their interaction has a considerable influence on efficiency and is attributed in part to ETL degradation in organic light-emitting diodes.

Keywords Degradation mechanism · Electron-transporting layer · Molecular dynamics simulation · Quantum mechanical/molecular mechanical method · Marcus theory

1 Introduction

Organic light-emitting diodes (OLEDs) have recently been used as displays in cell phones, televisions, electronic paper, and illuminations. In these OLEDs, emission is triggered by charge recombination of electrons and holes in the light-emitting layer (EML). Since the first report, in 1987, by Tang et al. [1] of a thin-layered structural device, the structures of OLEDs have been optimized for higher efficiency. For instance, tris(8-hydroxyquinolinate)aluminum (Alq_3), LiF, and Al are typical constructions for the electron-transporting layer (ETL) [2], electron-injecting layer, and cathode [3], respectively.

The Alq_3 molecule has geometrical isomers, meridional (*mer*-Alq_3), and facial (*fac*-Alq_3). Curioni et al. [4] have suggested that *mer*-Alq_3 is more stable than *fac*-Alq_3 by ca. 4 kcal/mol on the basis of their BLYP calculations using plane-wave basis sets. Because of its thermodynamic stability, readily available *mer*-Alq_3 has been used in OLEDs [5–9].

Alkali or alkali-earth metals possessing low work functions are used to lower the injection barriers from the cathode to the organic layers. LiF has several advantages: the molecule possesses a large dipole moment and a low electron-injection barrier against an Al cathode, it has low Joule heating, and it inhibits the diffusion motion of Al atoms. However, it is known that this molecule reduces the light emission efficiency of OLED devices [10] as a function of time. This

Dedicated to Professor Shigeru Nagase on the occasion of his 65th birthday and published as part of the Nagase Festschrift Issue.

T. Asada · K. Ohta · S. Koseki
Graduate School of Science, Osaka Prefecture University, 1-1 Gakuen-cho, Nakaku, Sakai, Osaka 599-8531, Japan

T. Asada (✉) · T. Matsushita · S. Koseki
The Research Institute for Molecular Electronic Devices, Osaka Prefecture University, 1-1 Gakuen-cho, Nakaku, Sakai, Osaka 599-8531, Japan
e-mail: asada@c.s.osakafu-u.ac.jp

T. Matsushita
Chisso Petrochemical Corporation, Goi Reseach Center, 5-1, Goikaigan, Ichihara, Chiba 290-8551, Japan

phenomenon is usually explained by the penetration of by Li ions into ETL.

In amorphous phases, the hopping model [11–13] is considered to be appropriate for describing the electron transfer (ET) between neighboring molecules, in which two interacting molecules with different electronic states such as radical anionic and neutral states are rather weakly bound by van der Waals interactions. Using the hopping model, Lin et al. [11] have demonstrated that ET mainly occurs through quinoline moieties in *mer*-Alq_3. They used a simple energy splitting in dimer (ESID) method [14, 15] to evaluate transfer integrals between Alq_3 molecules. Since the molecular orientation of two molecules is not taken into consideration in the ESID method, it is difficult to estimate a reliable transfer integral in the amorphous layer. In order to understand relative configurations in the disordered structure of Alq_3 molecules, computer simulations were performed, such as kinetic Monte Carlo simulation [12] and quantum mechanical/molecular mechanical (QM/MM) molecular dynamics (MD) simulation [16]. Kwiatkowski et al. [12] have also analyzed the rate constants for electron and hole transfers in calculated structures and successfully reproduced the ratio of these rate constants obtained on the basis of experimental measurements for disordered Alq_3 systems. Yanagisawa et al. have calculated work functions using first-principle MD simulations in order to demonstrate that the energy barrier of an electron injection is reduced by the coordination of the Alq_3 molecule on a Mg surface [17].

On the other hand, the degradation process of ETL by the coordination of alkali metals or alkali-earth metals has not yet been clarified. Therefore, the present paper discusses the mechanisms of ET in an Alq_3 layer partially coordinated by a $(LiF)_4$ cluster. Since total energies cannot be properly evaluated using simple classical MM force fields, model structures in the amorphous layer are constructed using QM/MM MD simulation [18–20]. First, these model structures of the Alq_3 molecule in the amorphous layer are discussed when a $(LiF)_4$ cluster is coordinated. Then, using Marcus theory [21, 22], the rate constants of ET in an Alq_3 layer are estimated with and without the coordination of a $(LiF)_4$ cluster in the hopping model [11–13]. The degradation mechanism of ETL is proposed on the basis of the present results.

2 Computational methods

2.1 Model structure preparation

A number of relative configurations of Alq_3 molecules in the amorphous layer were generated using QM/MM MD simulations at room temperature. The initial configuration in a unit cell was prepared using the Leap module of the Amber9 package [23] to include 125 *mer*-Alq_3 molecules, in which MM force fields of the Alq_3 molecule are generated by the Antechamber module. An MM MD simulation was performed for 2,000 ps at a temperature of 1,000 K to generate random configurations under periodic boundary conditions. The time step in this simulation was taken as 1 fs. The system was gradually cooled to 300 K, and MM MD simulation was performed for an additional 1,000 ps under the assumption of an NVT ensemble at 300 K in order to equilibrate the system. Then, MM MD simulation under the condition of constant pressure was carried out for 2,000 ps to prepare a model structure in the amorphous layer at a pressure of 1 atm. The resulting model system has a mass density of 1.42 g/cm^3. This result is in good agreement with the experimental value of 1.38–1.42 g/cm^3 [24]. In addition, the diffusion constant of the present model system is calculated to be 1.08×10^{-11} m^2/s on the basis of the Stokes–Einstein equation and agrees reasonably with the experimental value of $3 \pm 1 \times 10^{-10}$ m^2/s [25]. Technically, this calculated diffusion constant is slightly smaller than the experimental value, but it was found to be improved to 3.3×10^{-10} m^2/s in subsequent QM/MM MD simulation (see next section).

A vacuum region with a length of 30 Å was added along one of the three directions in the unit cell obtained by the above MM simulation to employ it as a model for amorphous layers. In the following investigation, the direction is taken as the z axis. For the purpose of obtaining realistic coordination structures of LiF in the ETL, the QM/MM MD simulation for 12 ps was achieved by approaching a simple $(LiF)_4$ cluster on the prepared amorphous layer. The initial coordinate of the center of mass (COM) of the $(LiF)_4$ cluster was located ca. 12 Å apart from the COM of the nearest Alq_3 molecule. The temperature and pressure of the system were controlled at 300 K and 1 atm, respectively, and a time step of 1 fs was used for the QM/MM MD simulations.

2.2 QM/MM calculation

In the QM/MM calculation, the target system was divided into two regions, QM and MM. It was assumed that a $(LiF)_4$ cluster and its nearest Alq_3 molecule are included in the QM region and that other Alq_3 molecules belong to the MM regions in calculations of the present QM/MM MD simulation. To evaluate environmental effects on chemical properties, a charge-embedded approximation was applied for QM calculations. Accordingly, the electric fields produced by classical point charges in the MM region were included in the Hamiltonian of the QM region. The energy of the QM/MM system, E(QM/MM), can be expressed as

$$E(\mathrm{QM/MM}) = E(\mathrm{QM}) + E(\mathrm{MM}) + E(\mathrm{QM}\cdots\mathrm{MM}), \tag{1}$$

where E(QM) and E(MM) are total energies of the QM and MM regions, respectively, and E(QM···MM) are the interaction energies between QM and MM regions. When ψ is the wave function of electrons in the QM region, E(QM) can be written as

$$E(\mathrm{QM}) = \left\langle \psi \middle| -\frac{1}{2}\sum_i \nabla_i^2 + \frac{1}{2}\sum_{i\neq j}\frac{1}{r_{ij}} + \sum_{i,m}\frac{q_m}{r_{im}} - \sum_{i,a}\frac{Z_a}{r_{ia}} \middle| \psi \right\rangle + \frac{1}{2}\sum_{a\neq b}\frac{Z_a Z_b}{r_{ab}}, \tag{1}$$

where r_{ij} is the distance between the i-th and j-th electrons in the QM region, q_m is the point charge on the m-th atoms in the MM region, and Z_a is the nuclear charge on the a-th atom in the QM region. The first term consists of the sum of kinetic energies of electrons, electron–electron repulsions, electrostatic interactions between electrons in the QM region and point charges in the MM region, and electron–nuclear attractions. The second term is the sum of nuclear–nuclear repulsive interactions in the QM region. Thus, the molecular orbital (MO) in the QM region can be polarized under the external electric fields generated by MM charges, and the electrostatic interactions between polarized QM and MM regions are calculated by Eq. 2. In the present study, the M05/6-31G(d) method was used for the QM region using the Gaussian09 package [26]. The M05 functional has been developed by Truhler et al. [27] in order to improve the description of long-range interactions.

The total energy of the MM region, E(MM), can be expressed by classical force fields and non-bonded interactions as

$$E(\mathrm{MM}) = \sum_{\mathrm{bonds}} K_r\left(r - r_{\mathrm{eq}}\right)^2 + \sum_{\mathrm{angles}} K_\theta\left(\theta - \theta_{\mathrm{eq}}\right)^2 + \sum_{\mathrm{dihedrals}} \frac{V}{2}\left[1 + \cos(k\phi - \gamma)\right] + \sum_{m<n}\left[\frac{A_{mn}}{r_{mn}^{12}} - \frac{B_{mn}}{r_{mn}^{6}} + \frac{q_m q_n}{\varepsilon r_{mn}}\right]. \tag{3}$$

The first three terms are bonding energies, where r, θ, and ϕ are bond length, bond angle, and dihedral angle, respectively. The bond lengths and angles at the equilibrium structure are expressed by r_{eq} and θ_{eq}, respectively. Here, K_r and K_θ are force constants, and V, γ, and k are the energy barrier, phase shift, and periodicity of the potential for a specific dihedral angle, respectively. The final term shows the non-bonding interaction provided by 6–12 Lennard-Jones type of van der Waals interactions and electrostatic potentials between point charges in the MM regions, where A and B are van der Waals parameters, and r_{mn}, q_m, and ε are the distance between the m-th and n-th atoms, classical point charges on the m-th atom in the MM region, and the relative dielectric constant, respectively.

The interaction energy between the QM and MM regions is provided by the sum of the electrostatic interactions between point charges in the MM region and QM regions and the van der Waals interactions as

$$E(\mathrm{QM}\cdots\mathrm{MM}) = \frac{1}{2}\sum_{a,m}\frac{Z_a q_m}{r_{am}} + \sum_{a<m}\left[\frac{A_{am}}{r_{am}^{12}} - \frac{B_{am}}{r_{am}^{6}}\right]. \tag{4}$$

No electron–electron energies are included in this equation, since they are already included in Eq. 2.

2.3 Electron transfer rate constant

In the hopping model [11–13], the ET rate constant in the amorphous layer of Alq_3 is estimated by that between neighboring molecules. On the basis of semi-classical Marcus theory, the ET rate constant k_{e} can be expressed as

$$k_{\mathrm{e}} = \frac{4\pi}{h}\frac{t_{\mathrm{e}}^2}{\sqrt{4\pi\lambda_{\mathrm{e}}k_{\mathrm{B}}T}}\exp\frac{-(\Delta E_{\mathrm{e}} + \lambda_{\mathrm{e}})^2}{4\lambda_{\mathrm{e}}k_{\mathrm{B}}T}. \tag{5}$$

This equation includes the Planck constant h, the transfer integral t_{e}, the reorganization energy λ_{e}, the Boltzmann constant k_{B}, and the absolute temperature T, and the free-energy change is ΔE_{e} by ET between the two molecules. The reorganization energy can be evaluated by

$$\lambda_{\mathrm{e}} = \{E_-(Q_0) - E_-(Q_-)\} + \{E_0(Q_-) - E_0(Q_0)\}, \tag{6}$$

where $E_0(Q_0)$ and $E_-(Q_0)$ are the total energies of Alq_3 and its anionic radical, respectively, at the optimized structure Q_0 of Alq_3. Similarly, $E_0(Q_-)$ and $E_-(Q_-)$ are the total energies at the optimized structure Q_- of the anionic radical. Accordingly, the reorganization energy corresponds to the energy changes caused by the structural displacements caused by ET.

The transfer integrals t_{e} are computed by the procedure proposed by Valeev et al. [14, 15]. On the basis of the tight binding model, the Hamiltonian of the present system can be written as

$$H = \sum_m \varepsilon_m a_m^+ a_m + \sum_{m\neq n} t_{mn} a_m^+ a_n, \tag{7}$$

where a_m^+ and a_m are the creation and annihilation operators, respectively, and ε_m and t_{mn} are the electron site energy at the molecular site m and the transfer integral between molecular sites m and n, respectively.

In the MO calculation of a dimer, the following equation needs to be solved:

$$(H - ES)C = 0. \tag{8}$$

Here, H and S are the Hamiltonian and the overlap matrices, respectively, for a dimer "AB." These can be decomposed into two monomers (A and B) using two sets of orthogonalized MOs, ϕ^A and ϕ^B:

$$H = \begin{pmatrix} e_A & J_{AB} \\ J_{AB} & e_B \end{pmatrix} \tag{9}$$

and

$$S = \begin{pmatrix} 1 & S_{AB} \\ S_{AB} & 1 \end{pmatrix}, \tag{10}$$

where

$$e_A = \langle \phi^A | \hat{H} | \phi^A \rangle, \quad e_B = \langle \phi^B | \hat{H} | \phi^B \rangle, \\ J_{AB} = \langle \phi^A | \hat{H} | \phi^B \rangle, \quad S_{AB} = \langle \phi^A \mid \phi^B \rangle. \tag{11}$$

The elements of the partial matrices e and J are similar to the site and transfer integrals used in Marcus theory. When a set of MOs is optimized for a dimer, the partial orbitals corresponding to the two monomers are non-orthogonal to each other. Using the Löwdin symmetrical diagonalization method, the Hamiltonian matrix can be transferred into H^{eff}:

$$\mathbf{H}^{\mathbf{eff}} = \mathbf{S}^{-\frac{1}{2}}\mathbf{H}\mathbf{S}^{-\frac{1}{2}}. \tag{12}$$

In the ESID model [14, 15] based on Koopmans' theorem, ET integrals can be calculated from the energy splitting between the two lowest unoccupied molecular orbitals (LUMO and LUMO+1) in the dimer, $\Delta E_{\mathrm{LUMO,LUMO+1}}$:

$$t_{mn} = \Delta E_{\mathrm{LUMO,LUMO+1}}/2. \tag{13}$$

It is reasonable to suppose that LUMO and LUMO+1 in the dimer originate from the interaction between LUMOs in its component monomers. Thus, this equation may be a good approximation when the site energy splitting is close to zero and only when the LUMOs in both monomers play an important role in ET between the molecules.

3 Results and discussion

3.1 Model structure for the amorphous layer of Alq_3 with a $(LiF)_4$ cluster

Figure 1 shows the interatomic distances $R_{\mathrm{Li-O}}$ between four Li and O atoms in the nearest Alq_3 molecule along the 12 ps-QM/MM MD trajectory, where one of the three O atoms in the Alq_3 molecule was chosen, since the other two O atoms of the Alq_3 molecule are buried in the amorphous layer. At the early stage of this simulation, the Li atoms of the $(LiF)_4$ cluster approach the quinoline moiety of the Alq_3 molecule and then move to the O atom after thermal fluctuation of 5 ps at room temperature (purple line in Fig. 1). In the following discussion, the Alq_3 molecule coordinated by the $(LiF)_4$ cluster is denoted by Alq_3' in order to distinguish it from other Alq_3 molecules in the amorphous layer. First, for the purpose of analyzing the binding energies between Alq_3 and $(LiF)_4$, two types of coordination structure of the $Alq_3'(LiF)_4$ were chosen from the present QM/MM MD simulation and the interaction energies were analyzed (Fig. 2). One is a typical structure in the early stage of the coordination (1–4 ps), and the other structure is typically observed after the system reaches the equilibrated structure (>6 ps). These structures were optimized in vacuum at the MP2/LanL2DZ level of theory, and the binding energies were calculated with basis set superposition error (BSSE) corrections. The optimized structures are illustrated in Fig. 2, where their binding energies are described in the caption. As mentioned previously, the coordination to an O atom (Fig. 2b) is more favorable than that to a quinoline moiety (Fig. 2a) by 9.1 kcal/mol. Therefore, it is reasonable in the following discussion to employ the structure of the coordination to an O atom of Alq_3' at equilibrated structures. In fact, in the present investigation, several trajectories were obtained, all of which provide the equilibrated structures similar to that observed in this trajectory.

The final structure in the present QM/MM MD simulation was used to investigate ET mechanisms between Alq_3 molecules. In comparison with the optimized structure of an isolated Alq_3 molecule, the structure of Alq_3' is distorted

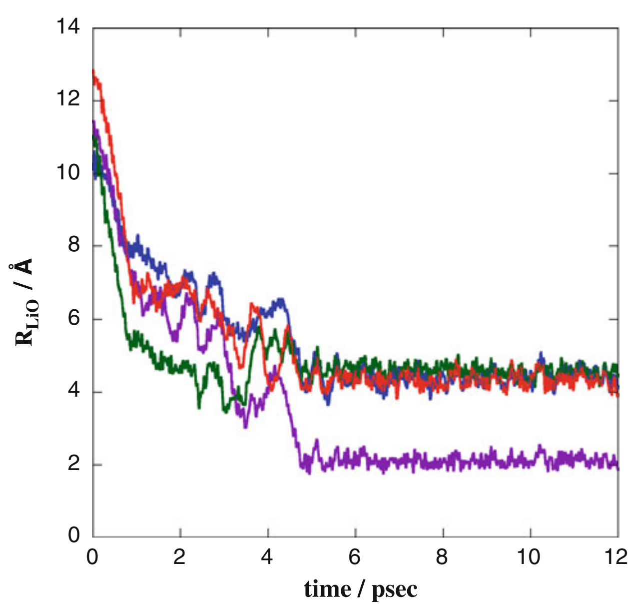

Fig. 1 All interatomic distances, $R_{\mathrm{Li-O}}$, between Li atoms and the closest O atom in the nearest Alq_3 molecule during 12 ps-QM/MM MD simulation. Each distance is drawn by the different *color*

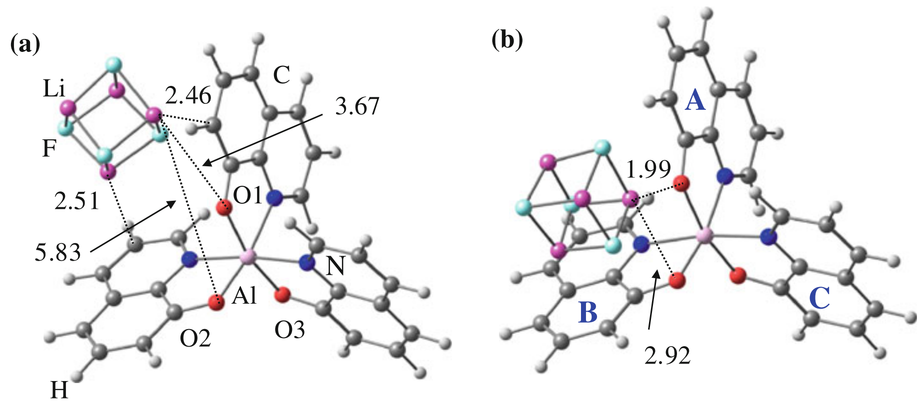

Fig. 2 Coordination structures of $Alq_3(LiF)_4$ molecules optimized from the snapshot of QM/MM MD simulation in the vacuum state at the MP2/LanL2DZ level of theory and interatomic distances in Å. The binding energies are evaluated at the MP2/LanL2DZ level of theory with basis set superposition error corrections. **a** $(LiF)_4$ binds to the quinoline *ring* with the binding energy of 8.6 kcal/mol. **b** $(LiF)_4$ binds to the oxygen atom with the binding energy of 17.7 kcal/mol

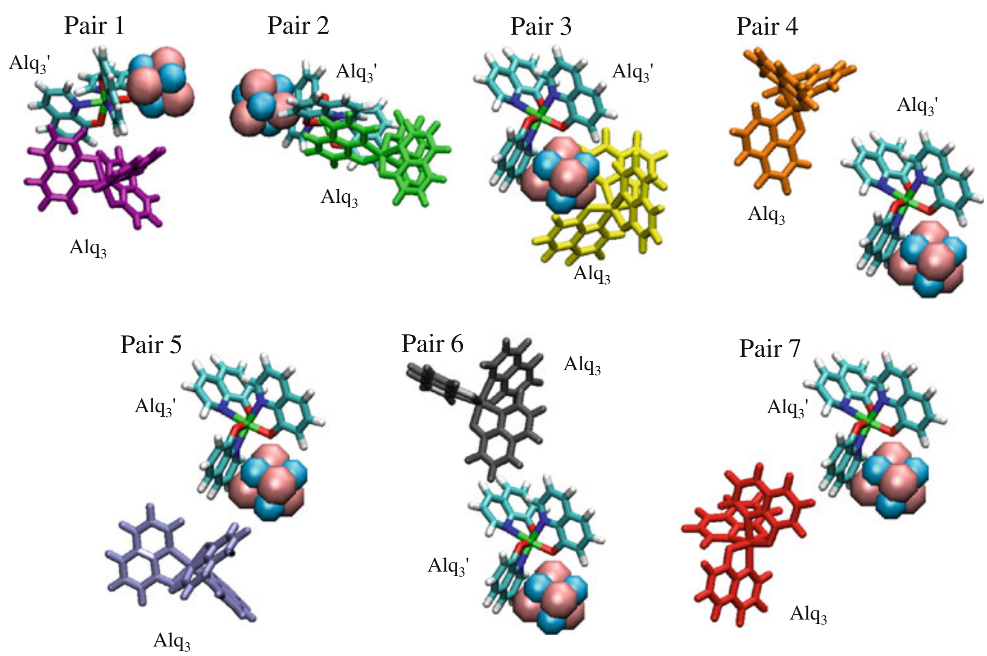

Fig. 3 Configuration of seven molecular pairs between $Alq_3'(LiF)_4$ and surrounding Alq_3 molecules at the 12 ps-snapshot taken from QM/MM MD simulation

by ca. 5° in both O2–Al–O3 and O1–Al–O3 angles (Fig. 2), and the twisted angle between the pyridine and phenyl rings of each quinoline moiety is calculated to be approximately 10 degrees. The number of Alq_3 molecules surrounding Alq_3' is found to be seven in the present simulation from analyzing the radial distribution in the amorphous layer. Figure 3 separately depicts seven configurations of Alq_3'–Alq_3 molecular pairs extracted from the final snapshot of the present simulation. Each pair is referred to as Pair i (i = 1–7) in the following discussion. Table 1 lists the geometrical parameters and the binding energies evaluated by the MP2/LanL2DZ method with BSSE corrections. The binding energy of the most stable pair (Pair 1) is found to be 7.4 kcal/mol, originating mainly from the π–π stacking interaction [28, 29] between the quinoline moieties. The intermolecular distance (R_c) between the COMs of Alq_3' and Alq_3 is calculated to be 7.11 Å. Although $R_c = 7.06$ Å in Pair 2, the binding energy is calculated to be 5.1 kcal/mol. It is considered that the number of π–π stacking pairs between quinoline moieties in Pair 2 is less than that in Pair 1, as shown in Fig. 3, and thus, the total interaction energy becomes rather weak.

Table 1 Binding energies, ΔE_{bind}, distances between center of mass, R_c, and the closest interatomic distance, r_{min}, between Alq_3' and Alq_3 molecules

Complex	ΔE_{bind}/kcal mol^{-1}	R_c/Å	r_{min}/Å
Pair 1	7.4	7.11	2.44
Pair 2	5.1	7.06	2.10
Pair 3	5.0	8.55	2.72
Pair 4	3.7	10.12	3.19
Pair 5	2.0	11.55	2.80
Pair 6	1.6	11.57	4.01
Pair 7	0.6	13.13	2.32

In the remaining pairs, R_c is calculated to be larger than 8.5 Å, and their binding energy is found to be less than 5.0 kcal/mol.

3.2 Theoretical analysis of electron transfer rate constants between Alq_3 molecules

In order to investigate the effects of LiF coordination on the Alq_3 amorphous layer, the rate constants, ET integrals, and reorganization energies were estimated for $Alq_3'\cdots Alq_3$ and for $Alq_3'(LiF)_4\cdots Alq_3$. In these analyses, all MO calculations were carried out at the M05/6-31G(d) level of theory.

3.3 Electron transfer rate constants between Alq_3 molecules

Table 2 summarizes the calculated properties relating to the rate constants of ET between Alq_3' and Alq_3. To examine the environmental effects on these properties, Pair 1, with the largest binding energy of all structures shown in Fig. 3, is optimized in vacuum, and the corresponding properties are also evaluated, as listed in Table 2. The binding energy in vacuum is approximately 10 kcal/mol more stable than that in the amorphous layer because of the distortion energy caused by the steric effects in the amorphous layer.

As mentioned previously, the π–π stacking interaction, which is mainly the result of charge-transfer interactions, is important between Alq_3 molecules. Although the charge-transfer interaction is based on the interaction between occupied and vacant MOs in each molecular pair, the transfer integral t_e is expected to show behavior similar to that of the charge-transfer interaction because both types of interaction are related to the overlap integrals between MOs, depending on the intermolecular distances. Since the optimized structure in vacuum favors a good π–π stacking interaction, it is reasonable to suppose that the transfer integral in the isolated complex is larger than that in the

Table 2 Reorganization energies, λ_e, transfer integral, t_e, site energy splittings, ΔE_e, rate constant of the electron transfer, k_e, and pair of molecular orbitals, MO(1)···MO(2), corresponding to the largest rate constant of the electron transfer $Alq_3'\cdots Alq_3$

Complex	λ_e/ meV	t_e/ meV	ΔE_e/ meV	k_e/s^{-1}	MO(1)···MO(2)
Pair 1	406	32	76	1.08×10^{11}	LUMO···LUMO+1
	310[a]	41[a]	173[a]	2.53×10^{10}[a]	LUMO···LUMO+1
	406[b]	21[b]	0[b]	2.33×10^{11}[b]	LUMO···LUMO
Pair 2	444	14	298	2.84×10^{7}	LUMO···LUMO+1
Pair 3	270	8	294	2.10×10^{5}	LUMO···LUMO+1
Pair 4	426	0.1	366	2.65×10^{2}	LUMO···LUMO
Pair 5	309	0.1	182	2.42×10^{5}	LUMO···LUMO
Pair 6	403	0.7	586	7.66×10^{-1}	LUMO···LUMO+3
Pair 7	3	0.1	211	6.75×10^{4}	LUMO···LUMO

[a] In the vacuum state

[b] Using ESID method

amorphous layer (See Table 2). Indeed, the overlap integrals for Pair 1 are 6.17×10^{-3} and 3.18×10^{-3} in vacuum and in the amorphous layer, respectively. Transfer integrals are significantly reduced for the other pairs with large intermolecular distances. However, in contrast to our calculated transfer integral of 32 meV, Difley et al. [16] have reported a largest transfer integral of 317 meV. A possible reason for this discrepancy is that our model structure is more disordered than theirs because they prepared it from crystal data using an MM molecular simulation technique, while ours was prepared by cooling from the gas phase. Our value is calculated to be 274 meV for the optimized structure in vacuum.

Although the reorganization energy λ_e of Pair 1 in the model amorphous layer appears to be larger than that of the optimized structure in vacuum by 0.1 eV, it is independent of the binding energies, as seen in Table 2. The present calculated values of 260–440 meV for the reorganization energy are similar to the range of 250–500 meV reported by Difley et al. On the other hand, the site energy splitting ΔE_e is affected by environmental factors. In the amorphous layer, the quinoline moieties are distorted because of steric hindrance by the surrounding molecules, as mentioned previously. If two molecules are symmetrically arranged in a dimer to give the same electronic state in each monomer, ΔE_e becomes zero. Therefore, ΔE_e in the crystal can be approximated to be zero, in contrast to that in the amorphous layer. The calculated values of ΔE_e are widely distributed from 76 to 586 meV, depending on the relative configuration of each molecular pair, where Pair 1 has the smallest value of all the molecular pairs. The larger the energy splitting, the smaller the rate constant, according to Marcus theory, given by Eq. 5. Some molecular pairs show larger values than those of 4–171 meV reported by Difley

Table 3 Transfer integrals, t_e, site energy splittings, ΔE_e, rate constants of the electron transfer, k_e, and overlap integrals, S, for some pairs of molecular orbitals in each monomer for the pair 1 in $Alq_3'\cdots Alq_3$

Alq_3'	Alq_3	t_e/meV	ΔE_e/meV	k_e/s^{-1}	$S\times10^{-3}$
LUMO	LUMO+1	32	76	1.08×10^{11}	3.18
LUMO	LUMO+2	25	348	2.11×10^{7}	1.99
LUMO	LUMO	11	33	3.26×10^{10}	0.11
LUMO+1	LUMO+1	17	38	7.25×10^{10}	2.54

et al., and this discrepancy is also explained by considering that the present model structure is more disordered than Difley et al.'s structure.

In considering the energies of MOs, it is reasonable to suppose that LUMOs are the dominant contributors to ET in the crystal, and thus, it is necessary to find the dominant pair of unoccupied MOs for the ET process for each pair since the energies and shapes of MOs vary in the amorphous layer. Table 3 shows the dependence of transfer integrals, site energy splittings, and rate constants of ET for various pairs of unoccupied MOs for Pair 1. Although the rate constant of ET between LUMOs is 3.26×10^{10} s^{-1}, the largest rate constant of 1.08×10^{11} s^{-1} originates from the interaction between LUMO and LUMO+1. Some unoccupied MOs in Pair 1 are shown in Fig. 4 for the dimer and for its component monomers, indicating that the shape of the low-lying LUMO in the $Alq_3'\cdots Alq_3$, denoted by LUMO($Alq_3'\cdots Alq_3$), has the character of both LUMO(Alq_3') and LUMO+1(Alq_3). Thus, it is reasonable to suppose that the rate constant in $Alq_3'\cdots Alq_3$ is described by the orbital interaction between LUMO(Alq_3') and LUMO+1(Alq_3). It is worth noting that ET can occur between some unoccupied MOs in each monomer; this consists of the low-lying delocalized unoccupied MO in the dimer.

3.4 Rate constants of electron transfer between Alq_3 molecules with a $(LiF)_4$ cluster

Table 4 summarizes calculated properties related to rate constants of ET between $Alq_3'(LiF)_4$ and Alq_3 molecules. The rate constant of ET for Pair 1 of $Alq_3'(LiF)_4\cdots Alq_3$ decreases compared with that of $Alq_3'\cdots Alq_3$, which is consistent with experimental results [10] that the coordination of LiF on the Alq_3 layer causes degradation of the ETL. However, when the ESID method is applied, the rate constant in $Alq_3'(LiF)\cdots Alq_3$ significantly increases to 4.60×10^{13} s^{-1}. Thus, the ESID method is not applicable for calculating the rate constant in the $Alq_3'(LiF)_4\cdots Alq_3$. In Pair 1, the unoccupied MOs in each monomer contributing to the large rate constant of ET become LUMO+2 and LUMO, in contrast to LUMO and LUMO+1 in $Alq_3'\cdots Alq_3$. Table 5 lists the dependences of transfer integrals, site energy splittings, and rate constants for some pairs of unoccupied MOs for Pair 1, used to evaluate the

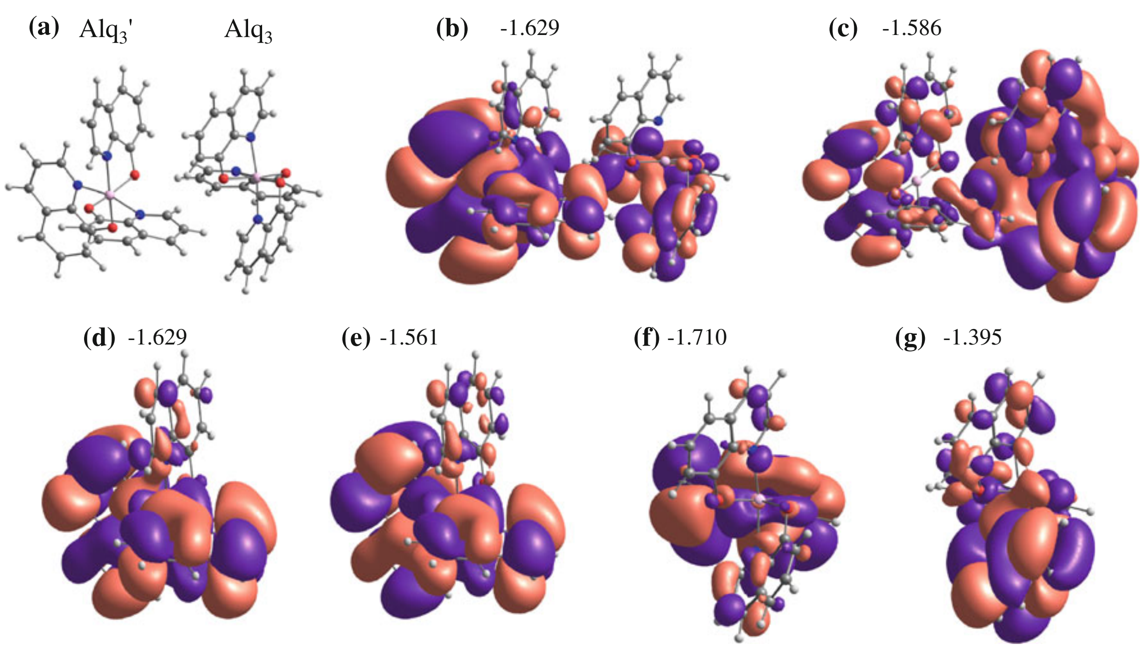

Fig. 4 Shapes and orbital energy in eV of molecular orbitals associated with the electron transfer between Alq_3 molecules. Values of the isosurface are 3.37×10^{-3} e/bohr^3 and 8.37×10^{-3} e/bohr^3 for the dimer and monomer, respectively. **a** Structure of $Alq_3'\cdots Alq_3$ for the pair 1. **b** LUMO in the $Alq_3'\cdots Alq_3$ dimer. **c** LUMO+1 in the $Alq_3'\cdots Alq_3$ dimer. **d** LUMO in the Alq_3' monomer. **e** LUMO+1 in the Alq_3' monomer. **f** LUMO in the Alq_3 monomer. **g** LUMO+1 in the Alq_3 monomer

Table 4 Reorganization energies, λ_e transfer integrals, t_e, site energy splittings, ΔE_e, rate constants of the electron transfer, k_e, and pair of molecular orbitals, MO(1)···MO(2), corresponding to the largest rate constant of the electron transfer for $Alq_3'(LiF)_4 \cdots Alq_3$

Complex	λ_e/ meV	t_e/ meV	ΔE_e/ meV	k_e/s^{-1}	MO(1)···MO(2)
Pair 1	294	9	24	9.23×10^{10}	LUMO+2···LUMO
	294	4	9	2.25×10^{10}	LUMO+1···LUMO
	294[a]	160[a]	0[a]	4.60×10^{13}[a]	LUMO···LUMO
Pair 2	408	11	301	2.14×10^{7}	LUMO···LUMO
Pair 3	426	8	522	2.35×10^{3}	LUMO···LUMO
Pair 4	214	2	382	1.26×10^{4}	LUMO···LUMO
Pair 5	361	0.4	549	1.15	LUMO···LUMO+2
Pair 6	314	4	373	2.30×10^{5}	LUMO···LUMO
Pair 7	291	0.4	254	2.55×10^{5}	LUMO+1···LUMO

[a] Using ESID method

Table 5 Transfer integrals, t_e, site energy splittings, ΔE_e, rate constants of the electron transfer, k_e, and overlap integrals, S, for some pairs of molecular orbitals in each monomer for the pair 1 in $Alq_3'(LiF)_4 \cdots Alq_3$

$Alq_3'(LiF)_4$	Alq_3	t_e/ meV	ΔE_e/ meV	k_e/s^{-1}	$S \times 10^{-3}$
LUMO+2	LUMO	9	24	9.23×10^{10}	1.05
LUMO+1	LUMO	4	9	2.25×10^{10}	0.30
LUMO	LUMO	5	354	7.29×10^{5}	0.46
LUMO	LUMO+1	10	439	5.92×10^{4}	1.31
LUMO+1	LUMO+1	17	289	1.28×10^{8}	2.22

rate constant for the other pair of MOs. While the rate constant of ET obtained from the interaction between LUMO+1($Alq_3'(LiF)_4$) and LUMO(Alq_3) is relatively large (2.25×10^{10} s^{-1}), the largest rate constant can be obtained between LUMO+2($Alq_3'(LiF)_4$) and Alq_3(-LUMO) in conjunction with both the large transfer integral and the small site energy splitting.

Figure 5 illustrates some low-lying unoccupied orbitals in the dimer and in its component monomers, $Alq_3'(LiF)_4$ and Alq_3. A drastic change can be found in the energy and shape of LUMO($Alq_3'(LiF)_4$), where the orbital energy of LUMO is lowered to −1.816 eV and the electron is clearly localized on quinoline moiety A (see Fig. 2b), far from the coordinated $(LiF)_4$ cluster, which is the distant quinoline moiety from the counter Alq_3 molecule. Since the energy of LUMO in the Alq_3 molecule is −1.407 eV, the energy separation of LUMOs between $Alq_3'(LiF)_4$ and Alq_3 molecules becomes large by the addition of $(LiF)_4$. Considering the perturbation method, the interaction between two MOs is inversely proportional to the orbital energy separation, which means that the interaction between LUMOs of $Alq_3'(LiF)_4$ and Alq_3 molecules becomes smaller than that of the $Alq_3' \cdots Alq_3$ because of the large orbital energy splitting. Therefore, the main character of LUMO($Alq_3'(LiF)_4 \cdots Alq_3$) is similar to that of LUMO($Alq_3'(LiF)_4$), and LUMO+1 and LUMO+2 in $Alq_3'(LiF)_4 \cdots Alq_3$ mainly originate from the orbital interaction between LUMO+1($Alq_3'(LiF)_4$) and LUMO(Alq_3), as seen in Fig. 5. In the ESID method, the transfer integral and thus the rate constant become large by

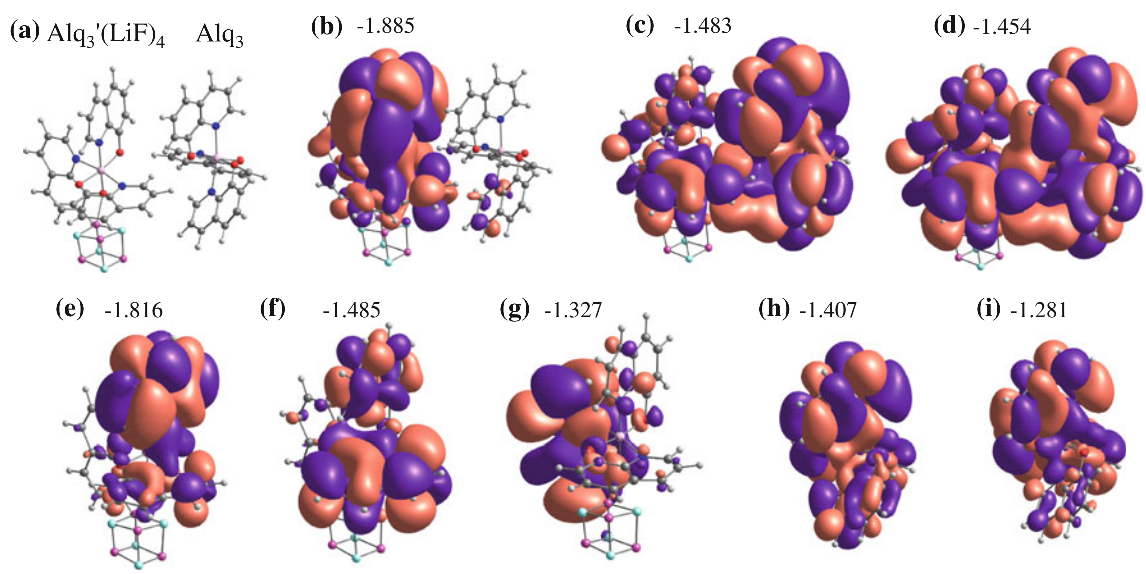

Fig. 5 Shapes and orbital energy in eV of molecular orbitals associated with the electron transfer between Alq_3 and $Alq_3(LiF)_4$ molecules. Values of the isosurface are 3.37×10^{-3}e/bohr^3 and 8.37×10^{-3} e/bohr^3 for the dimer and monomer, respectively. **a** Structure of $Alq_3'(LiF)_4 \cdots Alq_3$ for the pair 1. **b** LUMO in the $Alq_3'(LiF)_4 \cdots Alq_3$ dimer. **c** LUMO+1 in the $Alq_3'(LiF)_4 \cdots Alq_3$ dimer. **d** LUMO+2 in the $Alq_3'(LiF)_4 \cdots Alq_3$ dimer. **e** LUMO in the $Alq_3'(LiF)_4$ monomer. **f** LUMO+1 in the $Alq_3'(LiF)_4$ monomer. **g** LUMO+2 in the $Alq_3'(LiF)_4$ monomer. **h** LUMO in the Alq_3 monomer. **i** LUMO+1 in the Alq_3 monomer

coordination of $(LiF)_4$ because of the large energy separation between LUMO and LUMO+1 in the dimer.

Although an electron appears to be localized on quinoline moiety B (see Fig. 2b) for LUMO+2($Alq_3'(LiF)_4$) far from the Alq_3 molecule, the overlap integral of 1.05×10^{-3} between LUMO+2($Alq_3'(LiF)_4$) and LUMO(Alq_3) is larger than that between LUMO+1($Alq_3'(LiF)_4$) and LUMO(Alq_3), which is 3.0×10^{-4}. Thus, it is believed that the transfer integral increases between LUMO+2($Alq_3'(LiF)_4$) and LUMO(Alq_3). However, since the rate constant calculated from the orbital interaction between the pair of monomer unoccupied MOs does not depend on the orbital energy of the dimer, we must consider the energies of dimer orbitals and find a pair of suitable component monomer orbitals in order to calculate a reliable rate constant for ET. Since LUMO($Alq_3'(LiF)_4\cdots Alq_3$) is localized on quinoline moiety A in $Alq_3'(LiF)_4$, the delocalized LUMO+1($Alq_3'(LiF)_4\cdots Alq_3$) is considered to be an important MO for ET, which means that the rate constant for $Alq_3'(LiF)_4\cdots Alq_3$ is considered to be $2.25 \times 10^{10}\ s^{-1}$, obtained from the interaction between LUMO+1($Alq_3'(LiF)_4$) and LUMO(Alq_3) by coordination of $(LiF)_4$, rather than the largest rate constant of $9.23 \times 10^{10}\ s^{-1}$ between LUMO+2($Alq_3'(LiF)_4$) and LUMO(Alq_3).

On the basis of the present calculated results, we can propose a plausible degradation mechanism describing penetration of the Alq_3 amorphous layer by LiF. First, LUMO in Alq_3' becomes a stable localized orbital by coordination of the $(LiF)_4$ cluster, which does not play an important role in ET between Alq_3 molecules. Then, LUMO+1 becomes an important delocalized MO for ET with a relatively small rate constant, which may be related to degradation in the ETL. However, this preliminary investigation was performed for only those seven molecular pairs in the single configuration obtained from QM/MM MD simulations. Although our calculation could reproduce the small rate constants of ET for $Alq_3'(LiF)_4\cdots Alq_3$, the statistical average of calculated properties is yet to be compared with experimental measurements.

4 Conclusions

The mechanism of charge transfer in the ETL was analyzed on the basis of the hopping model and Marcus theory for a model Alq_3 amorphous layer generated by QM/MM MD simulation. A simple $(LiF)_4$ cluster was coordinated on the model amorphous layer for preliminary investigation of ET efficiency by penetration of the ETL by an LiF molecule from the electron-injection layer.

The QM/MM MD simulation indicates that the $(LiF)_4$ cluster favors coordinating with one of the O atoms in the Alq_3'. Since seven Alq_3 molecules can be found surrounding the Alq_3' molecule, the molecular pair with the largest rate constant of ET, denoted Pair 1, was selected for detailed theoretical analysis. Pair 1 also has the most favorable binding energy of 7.7 kcal/mol by π–π stacking interaction. Both ET and binding energies are related to the overlap integral between MOs, because the π–π stacking interaction originates from the charge-transfer interaction based on overlap integrals between occupied and vacant MOs, in addition to the fact that ET is related to overlap integrals between unoccupied MOs. The largest rate constant of ET without $(LiF)_4$ originates from the interaction between LUMO in the Alq_3 molecule and LUMO+1 in Alq_3', which is reasonable because LUMO in the $Alq_3'\cdots Alq_3$ dimer, denoted LUMO($Alq_3'\cdots Alq_3$), has the character of both LUMO+1(Alq_3') and LUMO(Alq_3).

The coordination of $(LiF)_4$ to Alq_3 reduces the rate constant of ET between Alq_3' and Alq_3 molecules to ca. 20% and drastically lowers the orbital energy of LUMO($Alq_3'(LiF)_4$). The electron in LUMO($Alq_3'(LiF)_4\cdots Alq_3$) is localized on the $Alq_3'(LiF)_4$ moiety because of the energy separation between LUMOs in $Alq_3'(LiF)_4$ and Alq_3 molecules. Therefore, LUMO in $Alq_3'(LiF)_4\cdots Alq_3$ cannot contribute to the ET, and thus, LUMO+1($Alq_3'(LiF)_4\cdots Alq_3$), whose component MOs are LUMO+1($Alq_3'(LiF)_4$) and LUMO(Alq_3), is considered to be an important MO for ET. The rate constant of ET between LUMO+1($Alq_3'(LiF)_4$) and LUMO(Alq_3) is calculated to be smaller than that without coordination of $(LiF)_4$. These results suggest that the penetration of the ETL by LiF considerably reduces the efficiency of electron transportation and is attributed in part to the degradation of the ETL in OLEDs.

Acknowledgments The first author (TA) acknowledges with sincere appreciation the financial support provided by Core Research for Evolution Science and Technology (CREST) "High Performance Computing for Multi-scale and Multi-physics Phenomena" from the Japan Science and Technology Agency. Part of this work was supported by Grant-in-Aid for Scientific Research (C) from the Japanese Ministry of Education, Culture, Sports, Science and Technology (No. 23550021).

References

1. Tang CW, VanSlyke SA (1987) Appl Phys Lett 51:913–915
2. Murata H, Malliaras GG, Uchida M, Shen Y, Kafafi ZH (2001) Chem Phys Lett 339:161–166
3. Hung LS, Zhang RQ, Mason PG (2002) J Phys D Appl Phys 35:103–107
4. Curioni A, Boero M, Adreoni W (1998) Chem Phys Lett 294:263–271
5. Baker BC, Sawyer DT (1968) Anal Chem 40:1945
6. Majer JR, Reade JA (1970) Chem Comm 1:58
7. Halls MD, Aroca R (1998) Can J Chem 76:1730–1736
8. Kushto GP, Iizumi Y, Kido J, Kafafi ZH (2000) J Phys Chem A 104:3670–3680
9. Brinkmann M, Gadret G, Muccini M, Taliani C, Masciocchi N, Sironi A (2000) J Am Chem Soc 122:5147–5157

10. Miyaguchi S, Ohata H, Hirasawa A (2007) Pioneer Res Dev 17:8–12
11. Lin BC, Cheng CP, You ZQ, Hsu CP (2005) J Am Chem Soc 127:66–67
12. Kwiatkowski JJ, Nelson J, Li H, Bredas JL (2008) Phys Chem Chem Phys 10:1852–1858
13. Fang XH, Hao YY, Han PD, Xu BS (2009) J Mol Struct:THEOCHEM 896:44–48
14. Valeev EF, Coropceanu V, da Silva Filho DA, Salman S, Bredas JL (2006) J Am Chem Soc 128:9882–9886
15. Coropceanu V, Cornil J, Da Silva Filho DA, Olivier Y, Silbey R, Bredas JL (2007) Chem Rev 107:926–952
16. Difley S, Wang LP, Yeganeh S, Yost SR, Voorhis TV, Accounts of Chemical Research 43:998–1004
17. Yanagisawa S, Morikawa Y (2009) J Phys:Condens Matter 21:1–6
18. Asada T, Hamamura S, Matsushita T, Koseki S (2009) Res Chem Intern 35:851–863
19. Asada T, Takahashi T, Koseki S (2008) Theor Chem Acc 120:85–94
20. Asada T, Nagase S, Nishimoto K, Koseki S (2008) J Phys Chem B 112:5718–5727
21. Marcus RA, Sutin N (1985) Biochemica et Biophysica Acta 811:265–322
22. Barbara PF, Meyer TJ, Ratner MA (1996) J Phys Chem 100:13148–13168
23. Case DA, Darden TA, Cheatham TE III, Simmerling CL, Wang J, Duke RE, Luo R, Merz KM, Pearlman DA, Crowley M, Walker RC, Zhang W, Wang B, Hayik S, Roitberg A, Seabra G, Wong KF, Paesani F, Wu X, Brozell S, Tsui V, Gohlke H, Yang L, Tan C, Mongan J, Hornak V, Cui G, Beroza P, Mathews DH, Schafmeister C, Ross WS, Kollman PA (2006) AMBER 9. University of California, San Francisco
24. Rajeswaran M, Blanton TN, Tang CW, Lenhart WC, Switalski S, Giesen DJ, Antalek BJ, Pawlik TD, Kondakov DY, Zumbulyadis N, Young RH (2009) Polyhedron 28:835–843
25. Priestley R, Walser AD, Dorsinville R (1998) Opt Commun 158:93–96
26. Frisch MJ, Trucks GW, Schlegel HB, Scuseria GE, Robb MA, Cheeseman JR, Scalmani G, Barone V, Mennucci B, Petersson GA, Nakatsuji H, Caricato M, Li X, Hratchian HP, Izmaylov AF, Bloino J, Zheng G, Sonnenberg JL, Hada M, Ehara M, Toyota K, Fukuda R, Hasegawa J, Ishida M, Nakajima T, Honda Y, Kitao O, Nakai H, Vreven T, Montgomery JA Jr, Peralta JE, Ogliaro F, Bearpark M, Heyd JJ, Brothers E, Kudin KN, Staroverov VN, Kobayashi R, Normand J, Raghavachari K, Rendell A, Burant JC, Iyengar SS, Tomasi J, Cossi M, Rega N, Millam JM, Klene M, Knox JE, Cross JB, Bakken V, Adamo C, Jaramillo J, Gomperts R, Stratmann RE, Yazyev O, Austin AJ, Cammi R, Pomelli C, Ochterski JW, Martin RL, Morokuma K, Zakrzewski VG, Voth GA, Salvador P, Dannenberg JJ, Dapprich S, Daniels AD, Farkas Ã, Foresman JB, Ortiz JV, Cioslowski J, Fox DJ (2009) Gaussian, Inc., Wallingford
27. Zhao Y, Schultz NE, Truhlar DG (2005) J Chem Phys 123:161103–161114
28. Baumeier B, Kirkpatrick J, Andrienko D (2010) Phys Chem Chem Phys 12:11103–11113
29. Lee EC, Kim D, Tarakeshwar P, Hobza P, Kim KS (2007) J Phys Chem A 111:3446–3457